RSC Advances

PAPER

View Article Online
View Journal | View Issue

Cite this: *RSC Adv.*, 2016, **6**, 63099

Polyaniline-intercalated layered double hydroxides: synthesis and properties for humidity sensing

Xiao-Zhou Li,[a] Shui-Ren Liu[a] and Ying Guo*[ab]

Received 19th April 2016
Accepted 15th June 2016

DOI: 10.1039/c6ra10093g

www.rsc.org/advances

A series of polyaniline and sodium dodecanesulfonate co-intercalated layered double hydroxides (LDH/PANI/SDS) have been obtained by a coprecipitation method. The composites have been named LiAl-LDH/PANI/SDS, MgAl-LDH/PANI/SDS, and NiAl-LDH/PANI/SDS according to the composition of the LDH nanosheets. The structure and chemical composition of the composites have been characterized by X-ray diffraction, Fourier transform infrared spectroscopy, scanning electron microscopy, transmission electron microscopy, thermogravimetry and differential thermal analysis. It has been observed that SDS serves as both the interlayer anion and the template for the formation of LDH sheets, which induces the co-intercalation of PANI. All the composites have been incorporated into humidity sensors and humidity sensing experiments have been conducted. It has been found that the humidity sensors based on LDH/PANI/SDS demonstrate good humidity properties with good linearity, low hysteresis, good stability and rapid response compared with PANI alone. The sensing mechanism of the composites has also been discussed.

1. Introduction

In recent years, the important issue of environmental humidity has caused extensive concern. Many efforts have been made to develop humidity sensors which have been widely used in environment control, food storage, industrial manufacturing, plant cultivation, *etc.*[1,2] As the main part of the sensitive layer, various inorganic and polymer materials have been studied for the development of humidity sensors. In general, metal oxides such as ZnO,[3] WO_3,[4] and TiO_2,[5] which have good chemical and thermal stability, have been widely utilized for humidity sensing. Additionally, polymers have gained more and more attention due to their characteristics of flexibility, low cost, wide range of relative humidity tests and simple fabrication processes.[6,7] Polyaniline (PANI), a conjugated conducting polymer, has been utilized for humidity sensing and exhibits good conductivity and electrochemical reversibility.[8,9] However, PANI shows the intrinsic shortcomings of instability at high humidity and high hysteresis.[10,11] To solve this problem, many references have reported the humidity properties of modified PANI composites. To a certain degree, the modified PANI composites showed better sensing performance in terms of response time, sensitivity and repeatability compared to unmodified PANI. Commonly used modifying methods include doping with metal oxides,[12] forming nanofibres,[13] and depositing ultrathin films.[14]

Because all inorganic and organic materials have advantages and disadvantages as humidity materials, it is desirable to obtain organic–inorganic composites, which maintain their respective advantages and reciprocally compensate for their deficiencies. Consequently, some composite materials made of inorganic–organic compounds have been reported as humidity sensors, such as $BaTiO_3$/RMX,[15] nano-sized SiO_2/poly-(2-acrylamido-2-methylpropane sulfonate)[16] and LiCl/poly-(3-hydroxybenzoic acid).[17] As can be seen, all of the above inorganic–organic composite materials show better humidity-sensitive properties than the single substances.

In this paper, a series of organic–inorganic composites based on LDH/PANI/SDS have been synthesized, where SDS serves as a co-intercalated anion to introduce PANI into the interlamellar space. Inorganic–organic composites which contain PANI as the organic part and layered double hydroxides (LDHs) as the inorganic part have been used to study the advanced humidity sensing properties introduced by the inorganic nanosheets. These inorganic matrices, layered double hydroxides (LDHs), whose structures can be generally expressed as $[M^{II}_{1-x}M^{III}_x(OH)_2](A^{n-})_{x/n}\cdot mH_2O$ (where M^{II} and M^{III} are divalent and trivalent metals, respectively, and A^{n-} is an n-valent anion), are important layered materials that show great versatility in terms of their chemical composition and their ability to build 2D-organized structures. The stacking of the layers gives rise to an accessible interlayer space on the nanometer scale.[18,19] To the best of our knowledge, this is the first ever attempt to introduce

[a]*State Key Laboratory of Chemical Resource Engineering, Beijing University of Chemical Technology, P.O. Box 98, Beijing, 100029, P. R. China. E-mail: guoying@mail.buct.edu.cn; Tel: +86-10-64412115*

[b]*Beijing Key Laboratory of Environment Harmful Chemical Analysis, Beijing University of Chemical Technology, Beijing, 100029, P. R. China*

LDHs into the humidity sensing field; it is found that the LDH/PANI sensors exhibit high humidity sensitivity, rapid response and good stability compared with PANI alone. The incorporation of a humidity sensing polymer into the LDH gallery exhibits the following advantages: first, the LDH matrix provides the polymer molecules with a confined and stable environment, which improves their humidity and thermal stability; second, the polarizability and the transferability of the metal cations on the LDH sheets could enhance the interaction between the composites and water molecules and, hence, the impedance of the humidity sensors would decrease markedly with increasing RH.

2. Experimental

2.1. Materials

All chemicals used were analytical reagent (AR) grade. Polyaniline (PANI) and *N*-methyl-2-pyrrolidinone (NMP) were purchased from Sigma-Aldrich. Dimethyl formamide (DMF), sodium dodecanesulfonate (SDS, $C_{12}H_{25}SO_3Na$), lithium nitrate ($LiNO_3$), aluminum nitrate nonahydrate ($Al(NO_3)_3\cdot 9H_2O$), nickel nitrate hexahydrate ($Ni(NO_3)_2\cdot 6H_2O$), magnesium nitrate hexahydrate ($Mg(NO_3)_2\cdot 6H_2O$) and sodium hydroxide (NaOH) were purchased from Beijing Chemical Reagents Co.

2.2. Synthesis of LDH–PANI/SDS powder

Solution A: metal nitrate (12 mmol, monovalent or divalent metal cation) and $Al(NO_3)_3\cdot 9H_2O$ (4 mmol, trivalent metal cation) were dissolved in 60 mL of deionized water. (The metal nitrates were lithium nitrate, aluminum nitrate nonahydrate, and nickel nitrate hexahydrate, respectively.)

Solution B: 0.2 M NaOH solution.

Solution C: a blend of SDS (4 mmol) dissolved in 50 mL deionized water and PANI (0.1 g) dissolved in 50 mL DMF.

Typically, the synthesis of LiAl-LDH/PANI/SDS was carried out as follows: solution A and solution B were simultaneously added dropwise to solution C; the final pH of the aqueous solution was adjusted to 10.5 with solution B. The resulting gel was transferred to an autoclave and aged at 100 °C for 18 h. The obtained material was centrifuged and washed with deionized water three times, then dried at 60 °C for 12 h. MgAl-LDH/PANI/SDS and NiAl-LDH/PANI/SDS were manufactured by similar processes, with final pH values of 10 and 9, respectively.

2.3. Preparation of humidity sensors

The resulting LDH/PANI/SDS composite was mixed with minimal *N*-methyl-2-pyrrolidinone (NMP) solvent to form a paste. Then the paste was dip-coated on ceramic substrate (4 mm × 6 mm × 0.5 mm) and fabricated with an interdigital array of Ag–Pt electrodes (the spacing between the Ag–Pt electrodes was 2 mm) to form a film with a thickness of about 200 μm; the film was then dried in air at 40 °C for 6 h.

2.4. Measurements

Powder X-ray diffraction (XRD) data were collected on a Rigaku XRD-6000 diffractometer at 40 kV and 30 mA in the 2θ range of 3–70°. The morphologies of the samples were observed using a Zeiss SUPRA 55 instrument at 20 kV. The Fourier transform infrared (FTIR) spectra were recorded on a Bruker Vector-22 Fourier transform infrared spectrometer in the range of 4000 to 400 cm^{-1}. Thermogravimetry and differential thermal analysis (TG-DTA) were carried out using an HCT-1 thermal analysis system in the temperature range from 30 to 800 °C with a heating rate of 10 °C min^{-1} in air. Elemental analysis was performed using a Shimadzu ICPS-7500 inductively coupled plasma emission spectrometer (ICP). Carbon, hydrogen, nitrogen and sulfur analyses (C, H, N, and S) were carried out using a Vario EL Cube Analyzer.

The characteristic curves of humidity sensitive materials were measured using a CHS-1 intelligent test meter (Beijing Elite Tech. Co., Ltd., China). All the intercalated LDH materials were used to fabricate sensors to check their behavior for sensing humidity changes. The sensors were measured at room temperature and an AC voltage of 1 V, 100 Hz. Different humidities were provided by different saturated salt solutions of LiCl (11%), $MgCl_2$ (33%), K_2CO_3 (54%), NaCl (75%), KCl (85%), and K_2SO_4 (95%). At a certain humidity, the sensors were placed in a bottle for half an hour to enable the humidity source to reach equilibrium before measurement.

3. Results and discussion

3.1. Structures and morphologies

The X-ray diffraction (XRD) patterns of LiAl-LDH/PANI/SDS (a), MgAl-LDH/PANI/SDS (b) and NiAl-LDH/PANI/SDS (c) are shown in Fig. 1. The powder XRD patterns of the LDH/PANI/SDS samples exhibit narrow, strong (003), (006), (009) reflections, indicating the formation of the LDH structure.[20] The interlayer spacing can be calculated by averaging the positions of the three harmonics: $c = (1/3)(d_{003} + 2d_{006} + 3d_{009})$.[21] The (003) diffraction peaks of the three compounds appear at $2\theta = 3.50°$ (LiAl-LDH/PANI/SDS), 3.40° (MgAl-LDH/PANI/SDS), and 3.49° (NiAl-LDH/PANI/SDS). Compared with CO_3^{2-} intercalated LiAl-LDH,[22] the characteristic (003) peak of LiAl-LDH/PANI/SDS is shifted from $2\theta = 11.78°$ to 3.50°, which indicates the interlamellar space has been expanded by the guest molecules of PANI and SDS. Taking the thickness of the LDH layer as 0.48 nm (ref. 23) and the chain length of the $C_{12}H_{25}SO_3^-$ anion as 1.85 nm,[24] the basal spacing of the intercalated LDH is calculated to be about 2.33 nm if $C_{12}H_{25}SO_3^-$ is arranged in a monolayer. In our case, the basal spacing of the three composites can be obtained by the Bragg

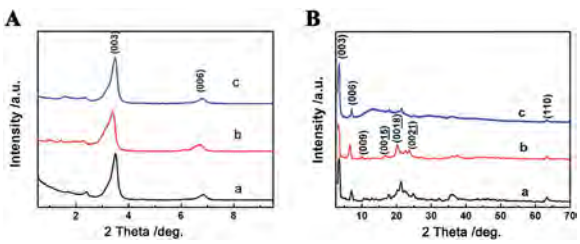

Fig. 1 Low angle (A) and wide angle (B) XRD patterns of (a): LiAl-LDH/PANI/SDS, (b): MgAl-LDH/PANI/SDS, (c): NiAl-LDH/PANI/SDS.

Table 1 Chemical compositions of the LDH/PANI/SDS samples

Sample	Chemical composition	M/Al ration (M = Li, Mg or Ni)
LiAl-LDH/PANI/SDS	$Li_{1.092}Al_{0.390}(OH)_2(C_{12}H_{25}SO_3)_{0.263}(C_{12}H_{12}N_2)_{0.084}$	2.8
MgAl-LDH/PANI/SDS	$Mg_{0.744}Al_{0.256}(OH)_2(C_{12}H_{25}SO_3)_{0.256}(C_{12}H_{12}N_2)_{0.091}$	2.9
NiAl-LDH/PANI/SDS	$Ni_{0.714}Al_{0.286}(OH)_2(C_{12}H_{25}SO_3)_{0.286}(C_{12}H_{12}N_2)_{0.092}$	2.5

equation; they are 2.52 nm ($d_{LiAl\text{-}LDH/PANI/SDS}$), 2.59 nm ($d_{MgAl\text{-}LDH/PANI/SDS}$) and 2.53 nm ($d_{NiAl\text{-}LDH/PANI/SDS}$). All the basal spacings are slightly larger than 2.33 nm, which indicates that the SDS is arranged in a monolayer between the layered nanosheets. The increase of the interlayer spacing above 2.33 nm can be attributed to the co-intercalation of SDS and PANI. The variation of the interlayer spacing can be attributed to the different ratios of PANI and SDS. The compositions of the products from ICP and C, H, N, and S analyses are given in Table 1. It can be seen that the interlayer spacing increases upon increase of the PANI/SDS ratio. Moreover, the experiment ratio of M (M = Li, Mg, Ni) to Al in the materials is close to the initial nominal ratio, as expected, which indicates that there is almost no loss of the metal content during the synthesis.

Fig. 2 shows the SEM and TEM images of the LDH/PANI/SDS. The morphologies and microstructures of the three LDHs were observed by SEM. As shown in the SEM images, the LDH samples exhibit mainly cumulate nanoflake-like structures with curved or contorted edges. All the images reveal a size distribution of 200 to 400 nm for the LDH nanoplates. Further observation from the TEM images shows that the LDHs exhibit characteristic LDH platelets with a uniform size of 200 nm to 400 nm. The morphology result shows that the cointercalated materials are layered materials, which is consistent with the XRD analysis.

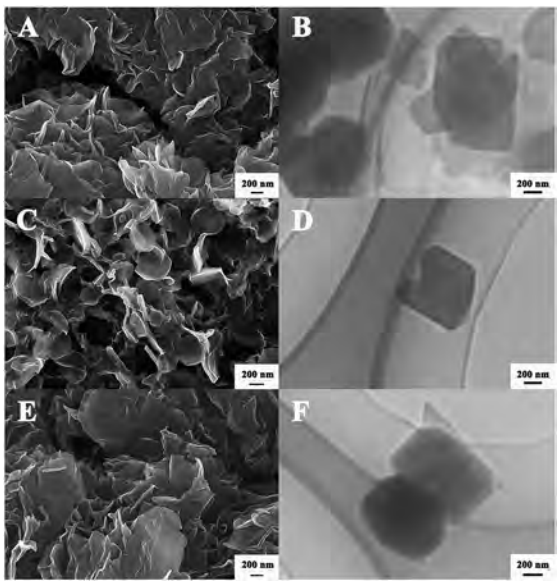

Fig. 2 SEM and TEM images of LiAl-LDH/PANI/SDS (A and B), MgAl-LDH/PANI/SDS (C and D) and NiAl-LDH/PANI/SDS (E and F).

Because PANI has no charge and has a certain chain length, it cannot be freely intercalated into the interlayer space. Therefore, anionic surfactants can sometimes be used as cointercalation molecules to assist the intercalation of the PANI molecules.[25] In our work, SDS is used as the interlayer anion to compensate for the positive charge of the hydroxide layers. In our paper, SDS is used to provide the PANI molecule with a homogeneous environment so as to enhance its humidity sensing properties.

As illustrated in Fig. 3, due to the strong electrostatic attraction between the surfactant anions and the metal cations, the metal cations can be adsorbed around the PANI and SDS anions to form layered structures where the SDS serves as interlayer anion and the template for the formation of LDH sheets. As discussed by Li *et al.*,[26] the growth of the LDH sheets can be induced to form curved or contorted morphologies by vesicles formed by superfluous SDS. There are two factors influencing the sheet contortion of sodium dodecanesulfonate intercalated LDHs. First is the weak interaction of layers through expanding the basal spacing, and second is the electronegative vesicles that electrostatically attract LDH layers and provide a bending force on the LDH layers. Finally, LDH grows into curved or contorted sheets, which are shown in the SEM image.

To further illustrate the structure and composition of these interlayered compounds, we take LiAl-LDH/PANI/SDS as an illustrative example. The IR spectra in Fig. 4 show the characteristic vibrations of PANI, SDS and the composite of LiAl-LDH/PANI/SDS. A broad absorption band of LiAl-LDH/PANI/SDS is

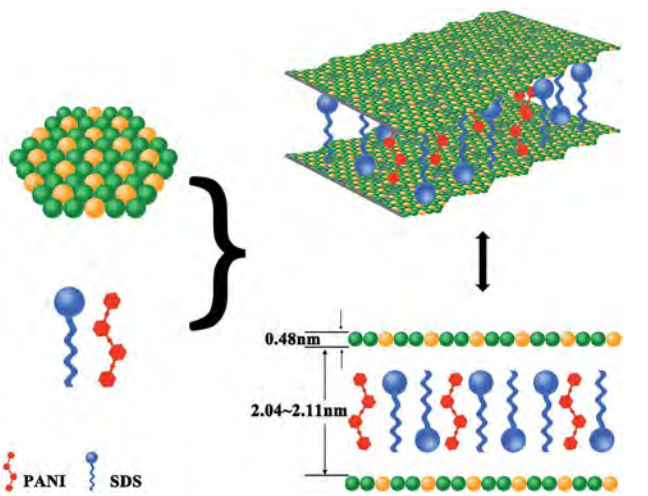

Fig. 3 Schematic of the formation of LDH/PANI/SDS.

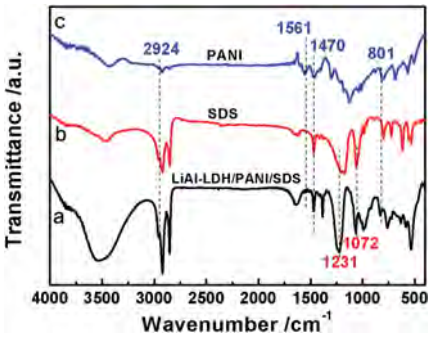

Fig. 4 IR spectra of LiAl-LDH/PANI/SDS (a), SDS (b) and PANI (c).

observed around 3500 cm^{-1}, which corresponds to the –OH stretching vibration. In addition to the –OH stretching vibrations, NH^{2+} stretching vibrations at 2924 cm^{-1} (NH^{2+} belongs to the $-C_6H_4NH^{2+}C_6H_4-$ group[27]), C=N vibrations at 1561 cm^{-1} (characteristic of the quinonoid units in PANI) and C=C vibrations at 1470 cm^{-1} (characteristic of the benzenoid units in PANI) are observed. This is attributed to the two states of polyaniline: the leuco-emeraldine salt state and the emeraldine salt state, which can be converted to one another under different conditions (Fig. 5). The peak at 801 cm^{-1} is assigned to the C–H bending vibration out of the plane of the *para*-disubstituted benzene rings.[28] The characteristic absorption peaks corresponding to the antisymmetric and symmetrical stretching vibrations of $-CH_2-$ from SDS are observed at 2919 and 2863 cm^{-1}. In addition, other characteristic bands, such as S=O antisymmetric (1231 cm^{-1}) and symmetric (1072 cm^{-1}) stretching vibrations, are also shown in the LiAl-LDH/PANI/SDS IR spectrum. All the vibration peaks of the composite indicate that PANI and SDS have been introduced in the composite successfully.

As shown in Fig. 6, the thermolysis behaviors of SDS, PANI and LiAl–PANI/SDS were studied. The DTA curve of SDS displays an exothermic effect at 150 °C, as well as a large exothermic peak with a maximum at 410 °C and a smaller peak at 490 °C. Meanwhile, the decomposition of PANI begins around 260 °C, with an exothermic effect. The DTA curve of LiAl-LDH/PANI/SDS shows that the decomposition process of the compound is an exothermic reaction, which is related to the decomposition and combustion of PANI and SDS. The TG curve of LiAl-LDH/PANI/SDS includes three stages: 160 to 230 °C, 230 to 330 °C and 330 to 550 °C. The weight loss in the temperature range of 160 to 230 °C is due to the desorption of structural water molecules and partial decomposition of SDS. A sharp weight loss in the range of 230 to 330 °C with a sharp exothermic peak in the DTA

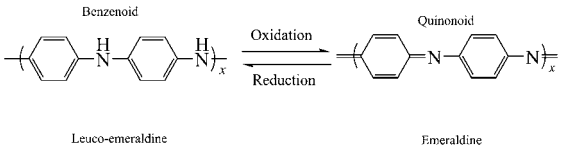

Fig. 5 Structures of PANI leuco-emeraldine salt and emeraldine salt.

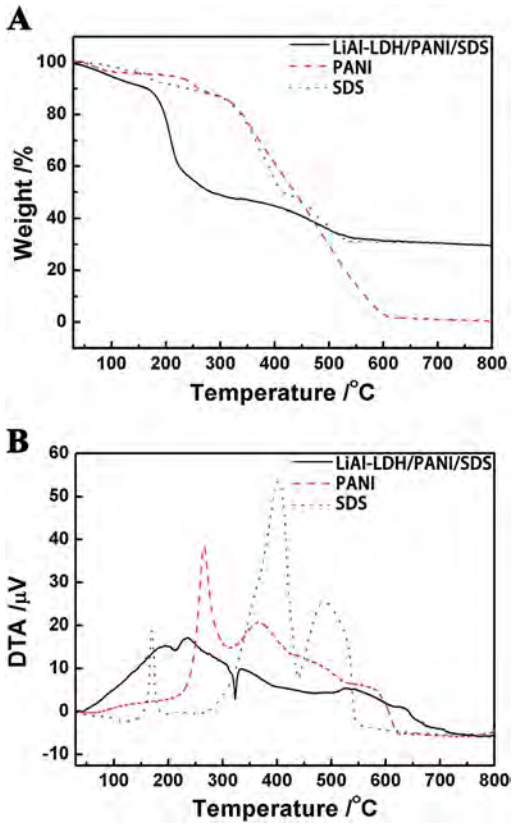

Fig. 6 TG (A) and DTA (B) curves for LiAl-LDH/PANI/SDS, SDS and PANI.

curve is mainly due to the decomposition of PANI. SDS and PANI continue to decompose when the compound is heated to 330 °C and give off a large amount of heat. Furthermore, the low peak of the LiAl-LDH/PANI/SDS DTA curve at 210 °C and 320 °C is due to the heat absorbed by further decomposition of the compound. Based upon this analysis, PANI and SDS have been intercalated into the gallery of the LDHs successfully.

3.2. Humidity sensing properties

The impedance of the sensor is seen to decrease as the level of relative humidity (RH) increases. When the sensing material is measured at increased or decreased RH, a hysteresis effort is observed. The humidity hysteresis characteristic of the LiAl-LDH/PANI/SDS composite is shown as a function of relative humidity in Fig. 7(A). It can be seen that the impedance changes from 185 to 3.7×10^5 kΩ, and the curve shows acceptable linearity. The differences between the humidification and desiccation processes in the range of 11% to 95% RH are within 5.2%. The response and recovery behavior are important characteristics for evaluating the performance of a humidity sensor. The time taken by a sensor to achieve 90% of the total impedance changes is defined as the response or recovery time.[29] Fig. 7(B) shows the response and recovery properties of the LiAl-LDH/PANI/SDS sensor between 11% and 95% RH. When the RH is increased from 11% to 95%, the response time of LiAl-LDH/PANI/SDS is less than 2 s. When the RH is decreased from

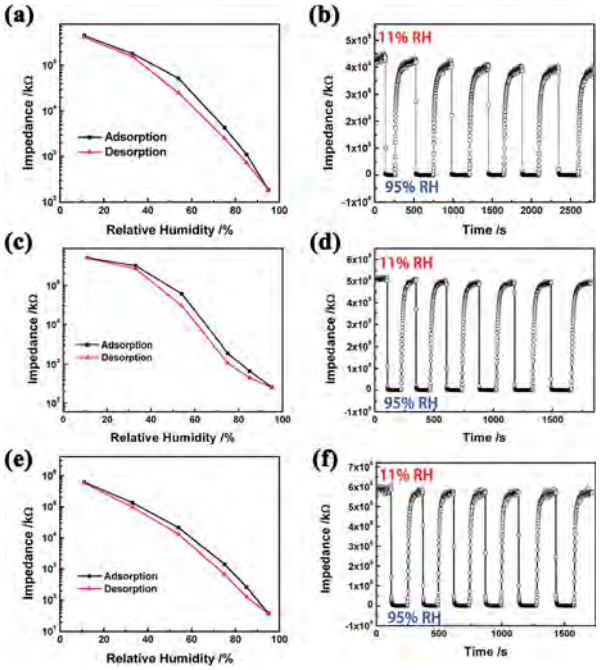

Fig. 7 Humidity hysteresis and response and recovery curves to humidity of LiAl-LDH/PANI/SDS (A and B), MgAl-LDH/PANI/SDS (C and D) and NiAl-LDH/PANI/SDS (E and F).

95% to 11%, the recovery time is about 30 s. It can be observed that LiAl-LDH/PANI/SDS exhibits good humidity sensing properties, such as quick response, high sensitivity and good linearity.

The humidity hysteresis and the response and recovery curve of MgAl-LDH/PANI/SDS are shown in Fig. 7(C) and (D), respectively. MgAl-LDH/PANI/SDS exhibits an impedance change of 3 orders of magnitude (5.1×10^5 to 258 kΩ) from 11% to 95% RH. Furthermore, the hysteresis is found to be about 4.5% under 54% RH. The response and recovery times of MgAl-LDH/PANI/SDS are calculated to be 3 s and 25 s, respectively.

The humidity hysteresis of NiAl-LDH/PANI/SDS is shown in Fig. 7(E). It can be clearly observed that NiAl-LDH/PANI/SDS exhibits a good sensing response as well. The impedance of NiAl-LDH/PANI/SDS changes linearly by four orders of magnitude (5.8×10^5 to 38 kΩ) from 11% RH to 95% RH on a semi-logarithmic scale, showing better linearity than LiAl-LDH/PANI/SDS and MgAl-LDH/PANI/SDS. The lines for the adsorption and desorption processes of NiAl-LDH/PANI/SDS are very close; the maximum humidity hysteresis is less than 3.2%. Also, from Fig. 7(F), we can see that the response and recovery times of NiAl-LDH/PANI/SDS are about 4 s and 25 s, respectively. All the measurements were repeated for seven cycles, as shown in Fig. 7, which indicates the good stability of the three samples for practical humidity sensing applications.

As shown above, the three humidity sensors of the series of LDH/PANI/SDS exhibit good sensing properties, such as ultrafast response time, good stability and good linearity. All three compounds are sensitive to humidity variations, and their response curves are similar. This ultrafast response behavior can be explained by the polarizability and the transferability of the metal cations.[30] When comparing the humidity sensitivity of the three samples, it is found that LiAl-LDH/PANI/SDS has the fastest response time and NiAl-LDH/PANI/SDS has the lowest humidity hysteresis. This is attributed to the difference in the cations, which leads to the slight difference in the humidity sensitivity of the three materials. The smaller the radius of the metal ions, the greater adsorption capacity for water molecules, and thus the fast response time; however, this also leads to higher hysteresis and slower water desorption. In addition, the LDH matrix provides polymer molecules with a stable environment, which ensures the good stability of the materials. All these results indicate that the chemical structures of the materials affect their sensing properties. The 2D-organized structure of LDH nanosheets is beneficial for improving the humidity sensitive properties and long-term stability of humidity sensors.

Sodium dodecanesulfonate (SDS) is an anionic surfactant which is not sensitive to humidity. Meanwhile, as a conjugated conducting polymer, polyaniline (PANI) exhibits high electrical conductivity and good humidity sensing linearity.[8] However, PANI normally shows intrinsic shortcomings of instability at high humidity and high hysteresis.[11] Also, PANI cannot recover its initial value after absorbing water, as can be seen from the response and recovery curve of PANI (Fig. 8); this is not beneficial for humidity sensing. Therefore, it is necessary to modify PANI to improve its humidity sensing stability. For comparison, the humidity curves of PANI and the PANI intercalated LDHs sensors have been shown in Fig. 9. As can be seen, within the whole humidity range, the impedance of the LDH sensors changes linearly by three or four orders of magnitude, while the impedance of PANI only decreases from 122 kΩ to 21 kΩ. The reason that LDHs possess high impedance at low humidity is that the interlayered PANI cannot easily absorb water at low humidity due to the confinement of the LDH platelets.

3.3. Discussion of the sensing mechanism

In order to study the mechanism of the humidity sensing behavior of the intercalated materials, complex impedance plots were measured from 10 Hz to 100 kHz at different RHs.

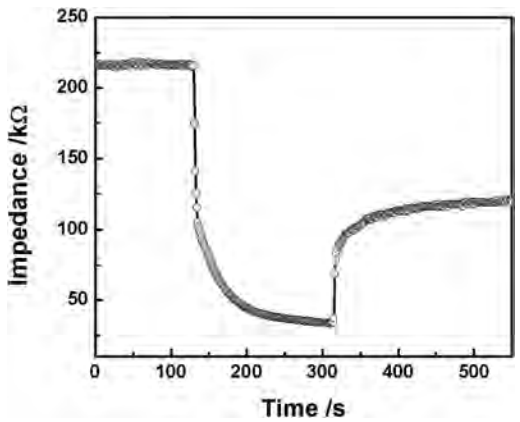

Fig. 8 Response and recovery curve to humidity of PANI.

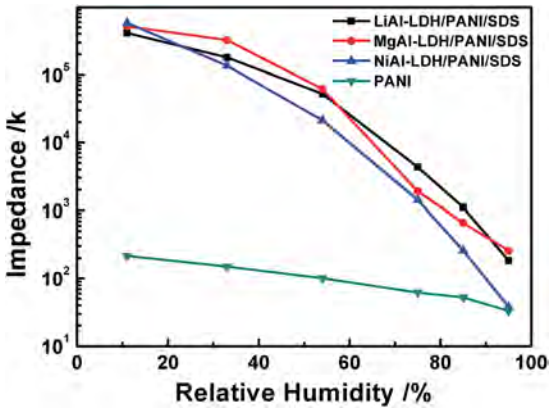

Fig. 9 Humidity curves of the LiAl-LDH/PANI/SDS, MgAl-LDH/PANI/SDS, NiAl-LDH/PANI/SDS and PANI sensors.

The complex impedance plots of LiAl–LDH/PANI/SDS are displayed in Fig. 10. Zr and Zi are the real and imaginary parts of the complex impedance plots, respectively. Because the LDH matrix provides polymer molecules with a confined and stable environment, the internal body electrons of the polymer have almost no contribution to the electronic conduction at 11% RH. The complex impedance plot appears to be an arc with a large curvature radius. Only a few water molecules are adsorbed on the surface of the LiAl-LDH/PANI/SDS composites, and the proton migrates by hopping from site to site across the material surface, resulting a relatively high impedance at 11% RH.[31] When the RH increases to 33% and 45%, a semicircle is observed in the complex impedance plot, which supports the existence of H^+ and H_3O^+ hopping conduction. In addition, it has been evidenced from NMR studies that this proton transfer from the polymer can take place in the presence of a water molecule.[32] The basic repeat units in PANI are characterized by the state of the nitrogen atom and are consequently labelled as NH_2^+ and NH. This transfer can be described by the following acid–base reaction:

$$NH_2^+ + H_2O \rightarrow NH + H_3O^+$$

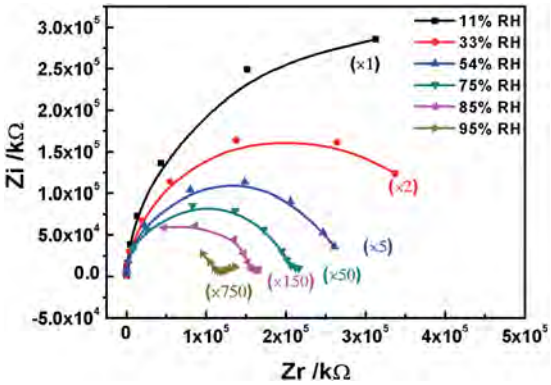

Fig. 10 Complex impedance of LiAl-LDH/PANI/SDS under different RHs and frequencies.

The role of water thus appears to be crucial for this mechanism.

As the RH further increased to 75%, 85% and 95% RH, the complex impedance plot comprised a partial semicircle at the high frequency range and a short line at the low frequency range. At high RH, a short line representing the Warburg impedance is observed, which is caused by diffusion of electroactive species at the electrodes.[33]

Jiang *et al.* reported the humidity sensing of Li-loaded microporous organic polymer assembled from 1,3,5-trihydeoxybenzene and terephthalic aldehyde;[34] they found that LiCl ionized to Li^+ and Cl^- at high humidity. In this work, we suspected that lithium cations could play the role of a conduction carrier which could transfer freely at high humidity. The polymer chain is attached to the LDH slab by weak van der Waals forces of attraction, and some Li cations are attached to the polymer chains and the LDH slab. When the RH is low (11%), only a few water molecules are absorbed on the surface of the LiAl-LDH/PANI/SDS composites, and the movement of Li ion is limited by the intermolecular forces, resulting in a relatively high impedance at 11% RH.[31] As the humidity increases, the materials absorb more water molecules; the chemisorbed water molecules are polarized to H^+, H_3O^+ and OH^-, and the transfer of H_3O^+ leads to a decrease in the impedance. Moreover, along with increasing RH (85%, 95%), the semicircle gradually disappears and the line lengthens. With the increase of adsorbed water molecules, several serial water layers are formed. As shown in Fig. 11, the quick transfer of Li ions on the water layers leads to an elongated straight line and results in a sharp decrease in the impedance of the sensor by three orders of magnitude compared with the initial impedance.

The complex impedance plots of MgAl-LDH/PANI/SDS (Fig. 12(A)) and NiAl-LDH/PANI/SDS (Fig. 12(B)) are similar to LiAl-LDH/PANI/SDS, which means that the humidity sensing mechanisms are similar. When the RH is low (<75%), a semicircle of film impedance is observed.[35] With increasing humidity, the semicircle gradually disappears and the line lengthens, indicating the diffusion of electroactive species. The quick transfer of metal cations on the water layers plays an important role in reducing the impedance.

The above results indicate that three humidity sensitive composites based on polyaniline-intercalated layered double

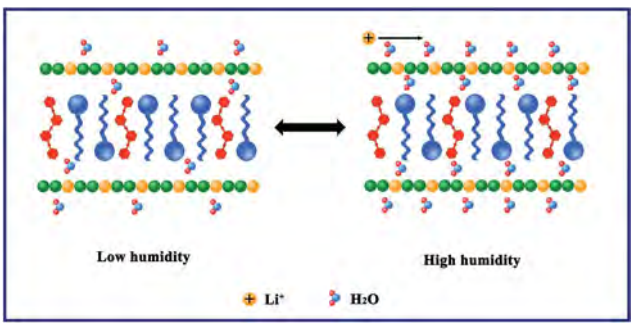

Fig. 11 The schematic of Li cation transportation at low humidity or high humidity.

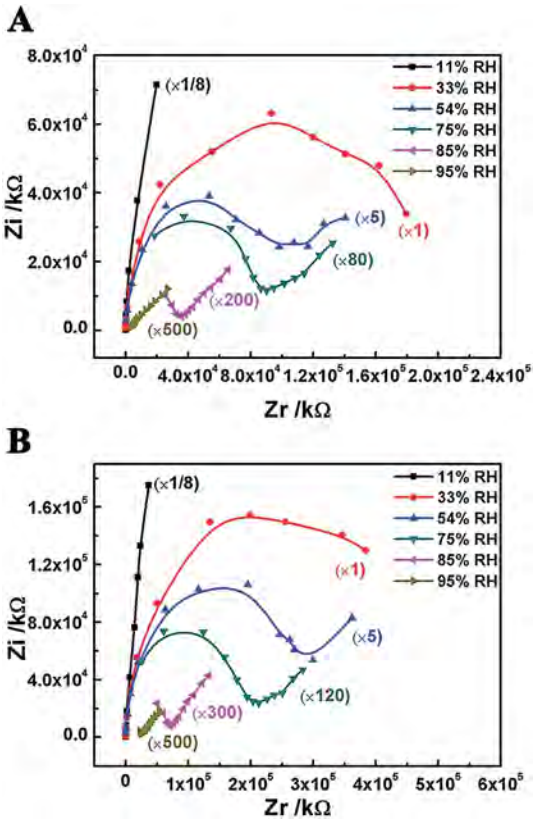

Fig. 12 Complex impedance of MgAl-LDH/PANI/SDS (A) and NiAl-LDH/PANI/SDS (B) under different RHs and frequencies.

hydroxides are obtained, with good linearity, low hysteresis, good stability and rapid response. All three composites exhibit similar humidity sensing mechanisms. As is known, PANI as a humidity sensitive material shows the intrinsic shortcomings of instability at high humidity and low hysteresis. The method of intercalating the polymer into an LDH matrix could enhance the humidity sensitivity properties of PANI, which seems to be a feasible approach to develop high performance humidity sensors.

4. Conclusions

In conclusion, a series of LDH/PANI/SDS composites with different metal cations were synthesized by co-intercalating polyaniline and dodecanesulfonate into the interlayer space of LDHs. Humidity sensors based on the LDH/PANI/SDS composites were fabricated and demonstrate good humidity properties, with good linearity, low hysteresis, good stability and rapid response. This is a novel method to fabricate organic–inorganic humidity materials with 2D-organized structures. The LDHs nanosheets play an important role in improving the long-term stability and humidity sensitive properties by providing a stable environment for the polymer and combining the metal cations on the LDHs nanosheets to improve the humidity response speed with polarized water molecules in the air. Because the structure of the materials strongly influences the sensing mechanism, further research on the design of materials with good sensitivity will be beneficial for device applications.

Acknowledgements

This study was supported by the National Natural Science Foundation of China (NSFC 51472021), the Scientific Research Foundation for the Returned Overseas Chinese Scholars, the State Education Ministry (LXJJ201302), the Fundamental Research Funds for the Central Universities (YS1406) and the Program for Changjiang Scholars and Innovative Research Team in University (IRT1205).

Notes and references

1 E. Bracken, *Sens. Rev.*, 1981, **17**, 291.
2 C. Y. Lee and G. B. Lee, *Sens. Lett.*, 2005, **3**, 1–15.
3 Q. Qi, T. Zhang, Q. J. Yu, R. Wang, Y. Zeng, L. Liu and H. B. Yang, *Sens. Actuators, B*, 2008, **133**, 638.
4 N. Parvatikar, S. Jain, S. Khasim, M. Revansiddappa, S. V. Bhoraskar and M. V. N. Ambika Prasad, *Sens. Actuators, B*, 2006, **114**, 599.
5 R. J. Wu, Y. L. Sun, C. C. Lin, H. W. Chen and M. Chavali, *Sens. Actuators, B*, 2006, **115**, 198.
6 F. W. Zeng, X. X. Liu, D. Diamond and K. T. Lau, *Sens. Actuators, B*, 2010, **143**, 530.
7 Y. Li and M. J. Yang, *Synth. Met.*, 2002, **129**, 285.
8 A. Alix, V. Lemoine, M. Nechtschein, J. P. Travers and C. Menardo, *Synth. Met.*, 1989, **29**, 457.
9 E. S. Matveeva, *Synth. Met.*, 1996, **79**, 127.
10 K. Ogura, T. Saino, M. Nakayama and H. Shiigi, *J. Mater. Chem.*, 1997, **7**, 2363–2366.
11 S. T. Mcgovern, G. M. Spinks and G. G. Wallace, *Sens. Actuators, B*, 2005, **107**, 657–665.
12 W. Geng, Q. Yuan, X. Jiang, J. Tu, L. Duan, J. Gu and Q. Zhang, *Sens. Actuators, B*, 2012, **174**, 513.
13 J. Gong, Y. Li, Z. Hu, Z. Zhou and Y. Deng, *J. Phys. Chem. C*, 2010, **114**, 9970.
14 R. Nohria, R. K. Khillan, Y. Su, R. Dikshit, Y. Lvov and K. Varahramyan, *Sens. Actuators, B*, 2006, **114**, 218.
15 J. Wang, Q. H. Lin, R. Q. Zhou and B. K. Xu, *Sens. Actuators, B*, 2002, **81**, 248.
16 P. G. Su and W. Y. Tsai, *Sens. Actuators, B*, 2004, **100**, 417.
17 K. Jiang, T. Fei and T. Zhang, *Sens. Actuators, B*, 2014, **199**, 1.
18 G. R. Williams, T. G. Dunbar, A. J. Beer, A. M. Fogg and D. O'Hare, *J. Mater. Chem.*, 2006, **16**, 1222.
19 W. Y. Shi, S. He, M. Wei, D. G. Evans and X. Duan, *Adv. Funct. Mater.*, 2010, **20**, 3856.
20 B. Wang, H. Zhang, D. G. Evans and X. Duan, *Mater. Chem. Phys.*, 2005, **92**, 190.
21 J. B. Zhou, Y. Cheng, J. G. Yu and G. Liu, *J. Mater. Chem.*, 2011, **21**, 19353.
22 J. P. Thiel, C. K. Chiang and K. R. Poeppelmeier, *Chem. Mater.*, 1993, **5**, 297.
23 M. Meyn, K. Beneke and G. Lagaly, *Inorg. Chem.*, 1990, **29**, 5201.
24 M. A. Drezdzon, *Inorg. Chem.*, 1988, **27**, 4628.

25 D. P. Yang, J. Lu, M. Wei, D. G. Evans and X. Duan, *J. Phys. Chem. B*, 2009, **113**, 1381.
26 B. Li and J. He, *J. Phys. Chem. C*, 2008, **112**, 10909.
27 G. D. Khuspe, D. K. Bandgar, S. Sen and V. B. Patil, *Synth. Met.*, 2012, **162**, 1822.
28 H. Tai, Y. Jiang, G. Xie, J. Yu, X. Chen and Z. Ying, *Sens. Actuators, B*, 2008, **129**, 319.
29 S. Agarwal and G. L. Sharma, *Sens. Actuators, B*, 2002, **85**, 205.
30 W. C. Geng, R. Wang, X. T. Li, Y. C. Zou, T. Zhang, J. C. Tu, Y. He and N. Li, *Sens. Actuators, B*, 2007, **127**, 323.
31 J. H. Anderson and G. A. Parks, *J. Phys. Chem.*, 1968, **72**, 3662.
32 S. Jain, S. Chakane, A. B. Samui, V. N. Krishnamurthy and S. V. Bhoraskar, *Sens. Actuators, B*, 2003, **96**, 124.
33 Y. Li, M. J. Yang and Y. She, *Talanta*, 2004, **62**, 707.
34 K. Jiang, T. Fei and T. Zhang, *RSC Adv.*, 2014, **4**, 28451.
35 C. D. Feng, S. L. Sun, H. Wang, C. U. Segre and J. R. Stetter, *Sens. Actuators, B*, 1997, **40**, 217.